Femtosecond TRIR Studies of ClNO Photochemistry in Solution: Evidence for Photoisomerization and Geminate Recombination†

Teresa J. Bixby, Joshua D. Patterson, and Philip J. Reid*

Department of Chemistry, University of Washington, Box 351700, Seattle, Washington 98195

Received: November 13, 2008; Revised Manuscript Received: December 16, 2008

The photochemistry of nitrosyl chloride (ClNO) in the solution phase is investigated using Fourier transform infrared (FTIR) and ultrafast time-resolved infrared (TRIR) spectroscopies. The NO-stretch fundamental transition for ClNO dissolved in cyclohexane, carbon tetrachloride, chloroform, dichloromethane, and acetonitrile is measured, with the frequency and line width of this transition demonstrating a strong dependence on solvent polarity. Following the photolysis of ClNO dissolved in acetonitrile at 266 nm, the subsequent optical-density evolution across the entire width of the NO-stretch fundamental is measured. Analysis of the optical-density evolution demonstrates that geminate recombination of the primary photofragments resulting in the reformation of ground state ClNO occurs with a quantum yield of 0.54 ± 0.06. In addition, an increase in optical density is observed at 1860 cm^{-1} that is assigned to the NO-stretch fundamental transition of the photoisomer, ClON, having a formation quantum yield of 0.07 ± 0.02. This work represents the first definitive observation of ClNO photoisomerization in solution. Finally, essentially no evidence is observed for significant vibrational excitation of the NO fragment following photodissociation, in marked contrast to the behavior observed in the gas phase. An environment-dependent dissociation scheme is proposed in which the interplay between solvent polarity and the location of the ground state potential-energy-surface minimum along the Cl−N coordinate provides for the optical preparation of different excited states thereby affecting the extent of NO vibrational excitation following photolysis.

Introduction

A significant challenge in atmospheric chemistry is to understand the fundamental aspects of phase-dependent photochemical reactivity. The environment-dependent reactivity of halooxides, such as chlorine dioxide (OClO), have attracted a significant amount of attention due to their role as a reservoir species for stratospheric atomic chlorine.[1−4] The recent discovery of a global stratospheric OClO layer has illustrated the importance of understanding the aspects that govern the potential of OClO and other halogen-containing species to release atomic chlorine.[5] Photoexcitation of gaseous OClO results primarily in the formation of OCl and O photofragments with a small amount of Cl and O_2 also formed.[6−8] However, production of the photoisomer, ClOO, has been observed in low-temperature matrixes,[9−12] and intermediate behavior with substantial formation of OCl/O, Cl/O_2, and photoisomer observed in solution.[13−23] Another halooxide, dichlorine monoxide (ClOCl), demonstrates photochemical behavior similar to OClO. While gaseous ClOCl forms ClO and Cl upon photoexcitation,[24−32] the isomer, ClClO, is produced in low-temperature matrixes. In solution, intermediate behavior is observed with geminate recombination of the ClO and Cl photofragments occurring in addition to ClClO formation.[10,33−37] To further investigate phase-dependent photochemistry in relatively simple molecular systems, we have initiated a series of studies involving nitrosyl halides, and in particular nitrosyl chloride (ClNO).[38]

Nitrosyl chloride is formed in the troposphere by the reaction of sea salt and NO_2 gas, and in the stratosphere by the reaction of HONO on frozen HCl surfaces.[39] The UV−vis absorption of ClNO is characterized by a series of bands, labeled the K through A as one proceeds from low to high energy, beginning ~650 nm and extending into the UV.[40,41] The A-band dominates the absorption spectrum, with a maximum in the absorption cross section occurring at 196 nm in the gas phase. Photoexcitation of gaseous ClNO resonant with the A-band results predominately in dissociation to form Cl and vibrationally excited NO.[42−54] The observation of vibrational energy in the NO photofragment up to $v = 7$ even at modest photolysis energies implies significant excited state evolution along the N−O stretch coordinate in the gas phase.[25,44,51−53,55] Only a few studies exist regarding the condensed phase photochemistry of ClNO. Low-temperature matrix isolation experiments on ClNO have observed a significant shift and broadening of the A-band absorption in comparison to the gas phase. Additionally, nearly exclusive formation of the photoisomer, ClON, following photoexcitation is observed.[12,56] In solution, broadening and bathochromic shifting of the A-band is observed, but the integrated intensity of the band remains constant indicating that no new transitions are being accessed. Resonance Raman intensity analysis studies demonstrated that excited state structural evolution in the A-band is dominated by the N−Cl stretch and bend coordinates. The increased broadening of the A-band with increased solvent polarity was attributed to an increase in the N−Cl bond length and corresponding shift of the ground state potential energy surface minimum along the N−Cl coordinate.[57,58] This assertion is supported by reduction in N−Cl stretch frequency with increasing solvent polarity. In contrast, the frequency of the N−O stretch does not undergo a significant frequency shift between the gas phase and argon matrixes. The resonance Raman studies found little scattering intensity along

† Part of the "George C. Schatz Festschrift".

* To whom correspondence should be addressed. E-mail: preid@chem.washington.edu.

10.1021/jp8100283 CCC: $40.75
Published on Web 02/11/2009

the N−O stretch consistent with modest excited state structural evolution along this coordinate upon photoexcitation.

To further investigate the condensed phase reactivity of ClNO following A-band photoexcitation, Cooksey et al. performed femtosecond pump−probe experiments on ClNO in solution.[38] These studies observed a photoinduced depletion of ClNO and subsequent photoproduct formation in all solvents studied: acetonitrile, chloroform, and dichloromethane. Photoproduct assignment and quantification of the geminate recombination quantum yield was hampered by overlapping absorption bands and assumptions of possible photoproduct locations based on data collected from matrix phases and other solvents. Modeling of the optical-density evolution in acetonitrile demonstrated that one photoproduct formed was the Cl:acetonitrile charge-transfer complex with quantum yield ∼0.55. However, the band shape and absorptivity of the photoproduct in chloroform was inconsistent with production of the Cl:chloroform charge-transfer complex. The photoproduct in chloroform was therefore assigned to the photoisomer.

Building on this previous pump−probe study, we report here static Fourier transform infrared (FTIR) and ultrafast time-resolved infrared (TRIR) studies designed to elucidate the environment-dependent photochemistry of ClNO. The IR absorption cross section of the N−O stretch fundamental of ClNO in various solvents was measured, and is observed to shift to higher energies and broaden significantly with an increase in solvent polarity. The evolution in optical density throughout the spectral region of the N−O stretch of ClNO in acetonitrile was monitored following A-band photoexcitation at 266 nm. Photoinduced depletion and subsequent geminate recombination of the primary Cl and NO photoproducts is observed, as well as the formation of a stable photoproduct. The geminate recombination quantum yield is determined to be 0.54 ± 0.06, consistent with earlier pump−probe work. The photoproduct is assigned to the structural isomer, ClON, with an associated quantum yield of ∼0.07. Little evidence is observed for vibrational excitation along the NO-stretch coordinate reinforcing the assertion that the energetics and displacement of the ground and excited states are significantly modified in solution relative to gas phase. In summary, the results presented here provide the first detailed insight into photoproduct formation and geminate recombination of ClNO in solution.

Experimental Section

A schematic of the femtosecond UV pump, IR probe spectrometer is presented in Figure 1. A Ti:sapphire oscillator (K&M Laboratories) pumped by the frequency-doubled output of a Nd:VO_4 laser (Coherent Verdi V) was used to seed a regenerative Ti:sapphire amplifier (Spectra Physics Spitfire). The output of the amplifier consisted of 50-fs pulses (full-width at half-maximum) centered at 800 nm with an energy of 1 mJ/pulse and repetition rate of 1 kHz. The amplifier output was split into two beams with a 60/40 beamsplitter. The higher energy beam was directed to an optical parametric amplifier (OPA, Quantronix TOPAS) to generate signal and idler fields at 1397 and 1895 nm, respectively. The signal and idler fields were overlapped in a $AgGaS_2$ crystal (type I) for difference frequency generation (DFG) producing the probe field centered at 5.35 μm with an energy of 1 μJ/pulse. The lower energy beam from the amplifier output was frequency-tripled using a series of β-BBO crystals (types I and II) to generate the 266-nm pump field.

The pump beam was delivered to a retroreflector mounted on a motorized delay stage (Newport ES300) to allow for

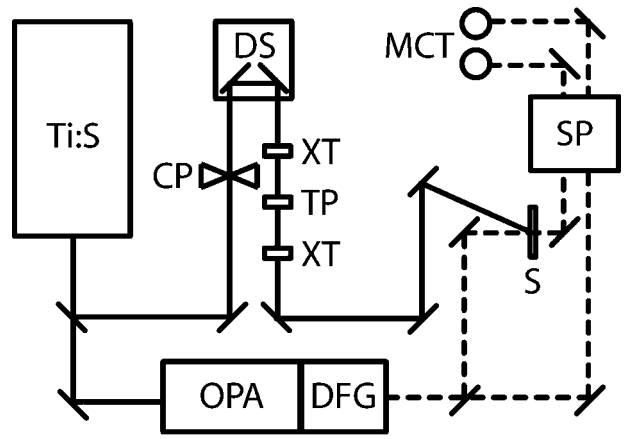

Figure 1. Schematic of the UV-pump, IR-probe spectrometer. Abbreviations are as follows: Ti:S, Ti:sapphire pumped regenerative amplifier; CP, mechanical chopper; DFG, difference frequency generator; DS, delay stage; MCT, mercury/cadmium/telluride detectors; OPA, optical parametric amplifier; S, sample cell; SP, spectrograph; TP, time plate; XT, β-BBO crystal.

temporal delay of the pump relative to the probe. Polarization of the pump beam was set to 54.7° relative to the probe by using a zero-order half-wave plate minimizing contributions from rotational dynamics to the observed optical-density evolution. The pump field (6 μJ/pulse) was weakly focused to a 1-mm diameter at the sample. The change in sample optical density was determined to be linearly dependent over a 5-fold change in pump power. Far field collimation of the 5.5-μm probe field was achieved using two off-axis parabolic mirrors (Janos). The collimated probe field was direct to a 50/50 CaF_2 beamsplitter with the reflected and transmitted beams corresponding to the signal and reference, respectively. The signal was focused on the sample using an off-axis parabolic mirror. Spatial and temporal overlap of pump and signal fields was verified by monitoring the change in optical density in a Si wafer following excitation at 266 nm. The observed optical response was modeled to establish an instrument time resolution of 200 fs.

After passing through the sample, the signal was delivered to a 0.25-m single-stage spectrograph (Jarrell Ash) equipped with a 100-groove/mm grating ($\lambda_{blaze} = 5.6$ μm). The reference arm also passed through the spectrograph, but vertically displaced from the signal. Identical components of the signal and reference fields were isolated with a spectral resolution of 4 cm^{-1}. Multiple orders of refracted light from a HeNe laser were used to calibrate the spectrograph, and further calibration was confirmed by taking the IR absorption spectrum of acetone and ClNO with our instrument and comparing this information directly to those obtained by a Bruker Vector 33 FTIR spectrometer with a demonstrated agreement of ±1 cm^{-1}. Upon exiting the spectrograph, the signal and reference were focused onto a pair of LN_2 cooled MCT detectors (Infrared Associates) with ZnO lenses. The output of each detector was sent to a gated integrator, and the integrator outputs were subtracted on a shot-to-shot basis. A mechanical chopper, placed in the pump field, was operated at half the repetition rate of the amplifier to block every other pump pulse. Successive probe signals were subtracted to determine the pump-induced change in optical density. Each recorded time point was averaged over 4000 laser shots, with each measurement consisting of the average of 3−7 time traces.

ClNO was prepared as described in the literature.[58] Briefly, 8.75 g of sodium nitrite dissolved in 12.5 mL of H_2O was added dropwise to 50 mL of concentrated hydrochloric acid. The

resulting ClNO gas was passed through a series of drying tubes packed with sodium nitrite, moist potassium chloride, and calcium chloride, then bubbled directly into a chilled flask containing the solvent of interest. The sample was delivered to a Teflon flow cell (Harrick Scientific) equipped with BaF_2 windows. BaF_2 windows were chosen instead of the more commonly used CaF_2 windows for their high damage threshold to aid in reducing coherent artifacts. Further, the focus of the pump beam was adjusted to minimize the coherence signal and solvent spectra indicate no evidence for this feature. A 100-μm cell path length was employed for TRIR studies involving transitions corresponding to ClNO, while studies involving the evolution in solvent vibrational modes were performed with use of a 56-μm path length. Sample concentrations, adjusted between 30 and 60 mM were verified using UV−vis absorption. Normalize of the resulting evolution in optical density was accomplished by dividing the probe intensity measured at the beginning and end of every scan. The absolute evolution in optical density was then analyzed by fitting the data scans to a sum of exponentials using the Levenberg−Marquardt algorithm. Goodness of fit was assessed by visual inspection of the residuals and reduced χ^2 values. The reported errors in extracted kinetic parameters represent one standard deviation of the mean determined from a minimum of 15 measurements. The variation in the absolute change in optical density among scans at a given wavelength is less than 10% and the data presented in Figure 3 represent an average of a minimum of 15 scans for each frequency.

The molar extinction coefficient of the NO-stretch fundamental transition of ClNO in the solvents of interest was determined using a Fourier transform infrared spectrometer (Bruker Vector 33). The ClNO samples were placed in an adjustable path length IR cell fitted with CaF_2 windows. Path lengths ranging from 300 to 400 μm were employed to ensure that measurements were below an absorbance of 1.0. Absorbance contributions from the solvent were removed by direct subtraction of the neat solvent spectra. Reported spectra were averaged over a minimum of 7 measurements.

Results

Absorption Spectra. The solvent-subtracted infrared absorption spectra of the NO-stretch fundamental (ν_1) transition of ClNO in cyclohexane, carbon tetrachloride, chloroform, dichloromethane, and acetonitrile are presented in Figure 2A. The absorption maxima in cyclohexane, carbon tetrachloride, chloroform, dichloromethane, and acetonitrile are located at 1805, 1815, 1836, 1845, and 1869 cm^{-1}, respectively. These data demonstrate that the transition shifts to higher frequency with an increase in solvent polarity. For reference, the $E_T(30)$ polarity-scale values are 30.9 (cyclohexane), 32.4 (carbon tetrachloride), 39.1 (chloroform), 40.7 (dichloromethane), and 45.6 kcal/mol (acetonitrile). A linear relationship between transition frequency and solvent polarity was observed (Figure 2B). Inspection of Figure 2A reveals that the shape and width of the transition are also solvent dependent. For example, in cyclohexane the line shape is Lorentzian with a width of 10.8 cm^{-1} at the full width at half-maximum (fwhm). However, as solvent polarity is increased the line shape becomes more Gaussian, and the breadth of the transition increases from 10.8 cm^{-1} in cyclohexane to 24 cm^{-1} in carbon tetrachloride, 44 cm^{-1} in chloroform, 43 cm^{-1} in dichloromethane, and 55 cm^{-1} in acetonitrile.

TRIR Studies of ClNO in Acetonitrile. The absolute evolution in optical density following ClNO photoexcitation dissolved in acetonitrile is presented in Figure 3. The range of

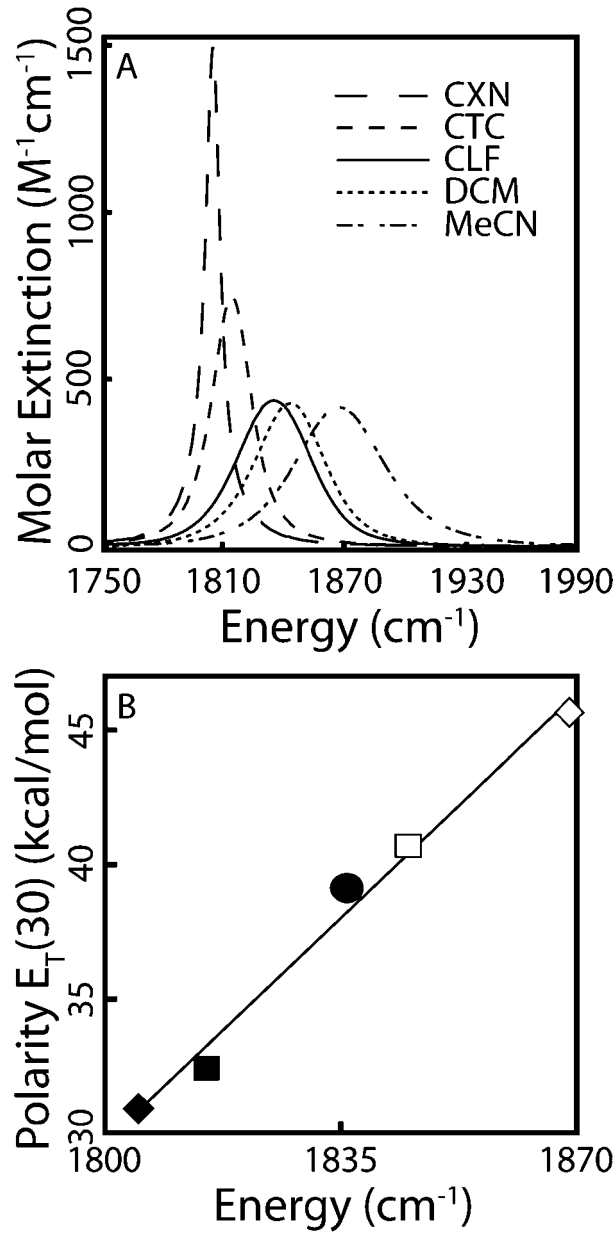

Figure 2. (A) IR absorption spectra of ClNO in the region of the NO-stretch fundamental transition in various solvents. (B) Plot of NO-stretch peak versus solvent polarity. Solvents are represented as follows: cyclohexane, CXN, filled diamond; carbon tetrachloride, CTC, filled square; chloroform, CLF, filled circle; dichloromethane, DCM, open square; acetonitrile, MeCN, open diamond.

probe frequencies (1820 to 1920 cm^{-1}) span the entire breadth of the NO-stretch fundamental transition (see Figure 2A). At all probe wavelengths a photoinduced reduction in optical density is observed consistent with photolysis of ground state ClNO. However, the temporal onset of this reduction varies across the absorption band. For frequencies between 1820 and 1840 cm^{-1}, an increase in optical density is observed prior to depletion suggesting that an absorptive species may be present on the low-energy side of the NO-stretch fundamental. The initial depletion of ground state ClNO is followed by partial optical-density recovery at all probe frequencies. Residual depletion in optical density remains constant out to the longest delay times investigated (90 ps), with amplitudes that vary from 30 to 56% across the band. The partial recovery in optical density following photoinduced depletion is indicative of geminate recombination of the primary photoproducts resulting

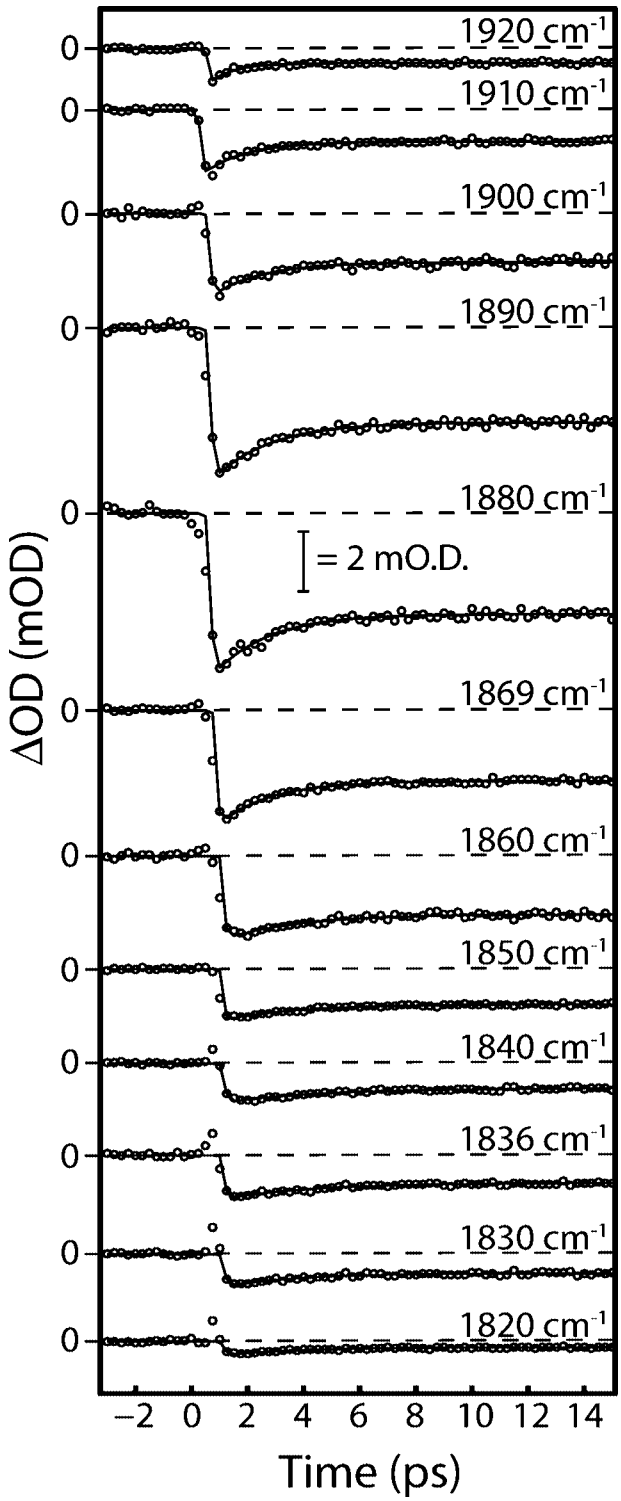

Figure 3. Evolution in optical density following photoexcitation at 266 nm of ClNO dissolved in acetonitrile. Probe frequencies at which the data was obtained are indicated. The circles represent the experimental data, while the solid lines correspond to the best fit to the data by a sum of exponentials with fit parameters provided in Table 1.

in ground state ClNO reformation. The best fit to the data was accomplished employing a sum of exponentials, with one exponential fixed at 10 000 ps to match the long-time offset in optical density. Time constants for recovery also vary across the band, ranging from 1.57 to 3.86 ps, with the fastest dynamics observed at higher probe energies and the slowest at lower probe energies. The kinetic parameters derived from fitting are presented in Table 1.

TABLE 1: Kinetic Parameters Determined from Analysis of TRIR Data for ClNO Dissolved in Acetonitrile

probe[a] (cm^{-1})	A_1[b]	τ_1 (ps)	A_2	τ_2 (ps)
1920	-0.47 ± 0.03	1.57 ± 0.19	-0.53 ± 0.03	$10\,000 \pm 0$
1910	-0.38 ± 0.02	1.85 ± 0.11	-0.62 ± 0.02	$10\,000 \pm 0$
1900	-0.44 ± 0.02	1.94 ± 0.11	-0.56 ± 0.02	$10\,000 \pm 0$
1890	-0.42 ± 0.03	2.05 ± 0.11	-0.58 ± 0.03	$10\,000 \pm 0$
1880	-0.38 ± 0.01	2.18 ± 0.14	-0.62 ± 0.01	$10\,000 \pm 0$
1869	-0.36 ± 0.01	2.54 ± 0.15	-0.64 ± 0.01	$10\,000 \pm 0$
1860	-0.31 ± 0.01	2.84 ± 0.19	-0.69 ± 0.01	$10\,000 \pm 0$
1850	-0.32 ± 0.03	2.84 ± 0.19	-0.68 ± 0.03	$10\,000 \pm 0$
1840	-0.36 ± 0.01	3.52 ± 0.23	-0.58 ± 0.06	$10\,000 \pm 0$
1836	-0.38 ± 0.02	3.86 ± 0.22	-0.62 ± 0.02	$10\,000 \pm 0$
1830	-0.39 ± 0.02	2.97 ± 0.24	-0.61 ± 0.02	$10\,000 \pm 0$
1820	-0.57 ± 0.02	3.27 ± 0.26	-0.43 ± 0.02	$10\,000 \pm 0$

[a] Wavelengths at which optical density evolution was measured. [b] Amplitudes are normalized such that $\sum|A_i| = 1$. Errors represent one standard deviation of the mean of all measurements (≥ 10) at a given probe wavelength.

The initial increase in optical density at lower probe energies combined with the frequency dependence of the time constant for ground state-depletion recovery warranted a more detailed analysis of the optical-density evolution. A second view of the optical-density evolution is provided by the two-dimensional contour plot shown in the top panel of Figure 4. The lower panel of this figure presents the infrared absorption spectra of ClNO dissolved in acetonitrile, as well as the deconvolved absorbance contributions from ClNO and acetonitrile over the spectral range investigated. The figure demonstrates that the absorbance over this region is dominated by the NO stretch fundamental transition (ν_1), with solvent contributing from 1820 to 1840 cm^{-1}. The solvent feature, centered at 1830 cm^{-1}, corresponds to the overtone of the acetonitrile C−C stretch. The top panel illustrates that the maximum reduction in optical density occurs at 1880 cm^{-1}, with most of the evolution completed within ~5 ps. Note that there is little to no evolution in the observed band shape despite the fact that it is asymmetric and the maximum of depletion does not converge to the maximum of the absorption band. As will be discussed later, the absence of band shape evolution is indicative of little to no excess vibrational energy being deposited into the NO stretch of geminately recombined ClNO.

Transient Absorption Spectrum. To further investigate the early time absorptive feature as well as the source of the asymmetric optical density depletion following excitation, the transient absorption spectrum of ClNO dissolved in acetonitrile was constructed from the contour plot in Figure 4. Taking "slices" along the time axis of the contour plot yields the transient absorption spectrum shown in Figure 5A. The asymmetry of the band and the shift in maximum reduction in optical density relative to the absorption peak are consistent with the presence of an optical density increase on the low-frequency side of the NO-stretch fundamental transition. To investigate this feature, the contribution of ground state ClNO depletion to the optical density evolution was determined using the high-frequency side of the NO stretch. The highest energy probe frequencies (1890 to 1920 cm^{-1}) exhibit behavior consistent with depletion and recovery of ground state ClNO exclusively. Therefore, the concentration of depleted ClNO was determined by these four frequencies, and its contribution was removed to construct the photoproduct spectra absorption presented in Figure 5B. To confirm the ability to decouple the photoproduct spectrum from the transient absorption spectra, subtraction of the predicted ClNO contribution was performed by using only the three highest probe energies, only the two highest probe

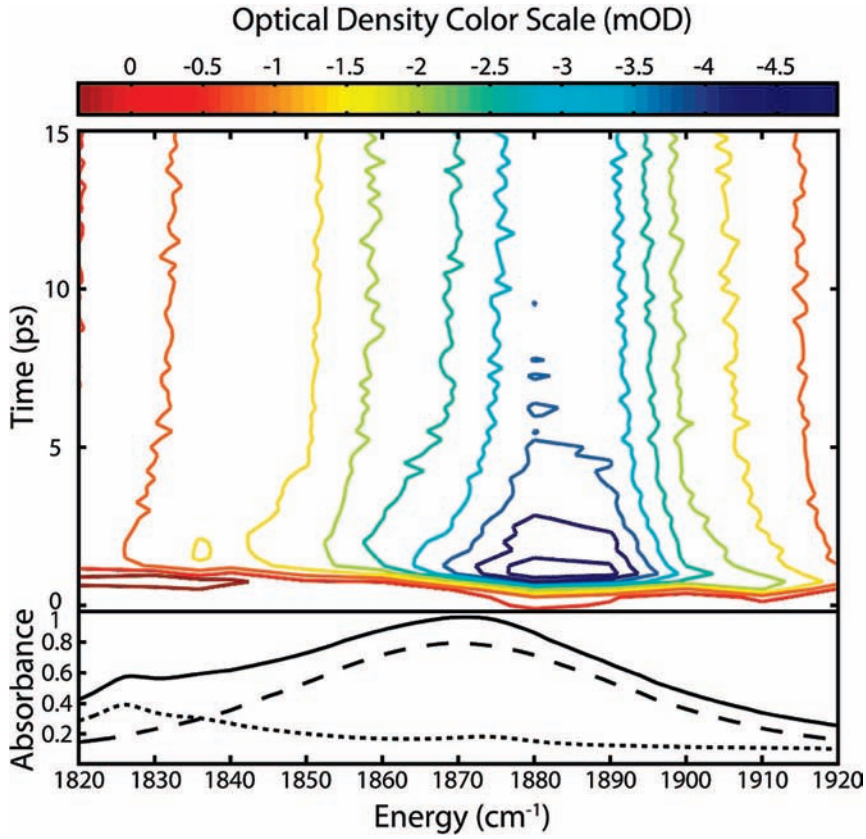

Figure 4. (Top) Contour plot of TRIR optical-density evolution observed in the NO-stretch fundamental of ClNO dissolved in acetonitrile. The absolute change in optical density is indicated by the contour lines, with the color scale shown above the plot. (Bottom) The IR absorption spectra of ClNO in acetonitrile (solid), acetonitrile only (short dashed), and the NO-stretch of ClNO (long dash).

energies, and only the highest probe energy. No difference in the position of any feature in the photoproduct spectrum appears and the absolute optical density changes less than 10%. The figure demonstrates an instrument-response-limited increase in optical density with subsequent decay to a constant positive offset within ~5 ps. The peak of the absorptive feature is at 1860 cm^{-1} and persists out to the longest delays investigated suggesting formation of a stable photoproduct. Additionally, a weaker absorption is seen to appear from 1820 to 1836 cm^{-1}, possibly signifying a change in absorptivity of the solvent transition. We will argue below that this behavior reflects formation of the chlorine−acetonitrile charge-transfer complex.

Discussion

ClNO Bonding in Solution. The central goal of this study was to investigate the condensed phase reaction dynamics of ClNO. Previous studies suggest that the reaction dynamics of ClNO may be significantly perturbed in solution relative to the gas phase as a consequence of solvent-induced structural changes, and thus changes in the electronic states, of ClNO.[58] For example, in the UV absorption spectrum of ClNO the strongest or "A-band" transition broadens and shifts from 198 nm in the gas phase to 206 nm in cyclohexane and 218 nm in acetonitrile. Comparison of the integrated intensity of the A-band in these solvents demonstrated that the overall intensity is conserved; therefore, the same electronic transitions are being accessed with excitation into this band. The increase in transition breadth with increasing solvent polarity was attributed to weakening of the N−Cl bond and a corresponding shift of the ground state potential-energy-surface minimum along the N−Cl stretch coordinate. This is consistent with the shift to lower energy of the absorption spectrum, and decrease in the N−Cl stretch and bending fundamental frequencies in polar solvents. Resonance Raman intensity analysis studies in both gas and solution phases observed modest to no evolution along the N−O stretch coordinate.[57−60] In addition, the N−O stretch frequency of ClNO in matrix phases is reported to lie within a few wavenumbers of gas phase measurements.[12,56,61,62] Those studies suggest that the environmental dependence of the N−O stretch is modest. However, we have demonstrated that the N−O stretch fundamental frequency increases from 1805 to 1869 cm^{-1}, broadens from 11 to 55 cm^{-1} at full-width at half-maximum (fwhm), and changes from a purely Lorentzian line shape to a more Gaussian line shape in going from cyclohexane to acetonitrile. It is apparent that ClNO undergoes dramatic structure modifications with environment, and these modifications should result in a corresponding change in the reaction dynamics in solution relative to the gas phase.

Insight into the nature of the NO-stretch solvent dependence is provided by considering theoretical descriptions of ClNO bonding. Ab initio SCF and CISD calculations predict that the N−Cl bond is extraordinarily long (1.973 Å) and the dipole moment of ClNO is large (2.49 D), consistent with substantial ionic character.[63,64] Furthermore, work by Meredith et al. describes the electronic structure of ClNO as a weak interaction between the singly occupied p orbital of Cl with the singly occupied 2π antibonding orbital of NO. The long N−Cl bond distance leads to poor overlap of these two out-of-plane orbitals and the high electronegativity of Cl results in a partial charge transfer from the NO to the Cl. This behavior results in an enhanced NO bond strength and bonding character similar to that of NO^+. These calculations also show that any perturbation

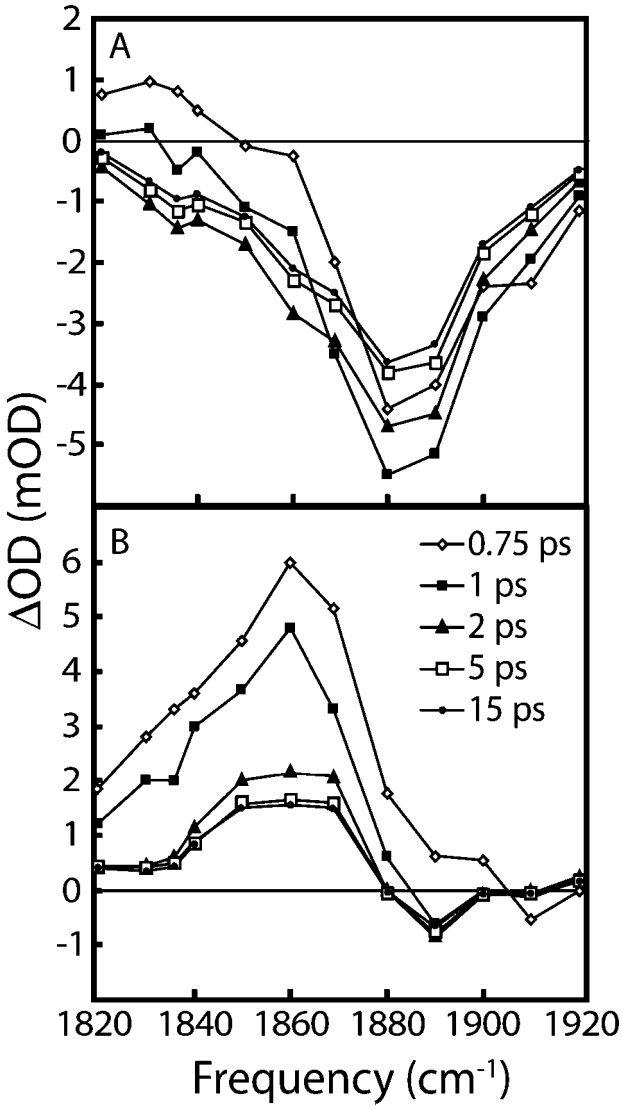

Figure 5. (A) Transient IR absorption spectrum of ClNO dissolved in acetonitrile. The time delay for each spectrum is given in the figure. (B) Transient IR absorption difference spectrum. Each spectrum is the difference between the measured absorption and the predicted ClNO absorption spectrum at each time delay.

such that there is increased separation between the N and Cl in the ground state enhances charge transfer making the NO bond more NO^+-*like*. The ionic nature of this interaction suggests that the N−Cl bond length and fundamental frequency will depend greatly on solvent polarity. This prediction is supported by frequency shifts observed in the resonance Raman spectrum where the frequency of the N−Cl fundamental decreases from 332 cm^{-1} in the gas phase to 325 cm^{-1} in cyclohexane and 310 cm^{-1} in acetonitrile.[58] In addition, Meredith's work predicts that the NO bond in ClNO should be stronger relative to molecular NO due to the charge transfer to the Cl p orbital reducing the population in the 2π antibonding orbital of NO. Other studies support this idea, placing the NO bond length in ClNO (1.13 Å) between that of molecular NO (1.162 Å) and NO^+ (1.078 Å).[63,64] We propose that an increase in solvent polarity weakens and lengthens the N−Cl bond and consequently enhances the extent of charge transfer from the 2π antibonding orbital of NO to the p orbital of Cl. The reduction of electron density in the antibonding orbital of NO subsequently shifts the bonding characteristics of the NO moiety closer to that of NO^+ with a corresponding increase in the vibrational frequency of the NO stretch. It is important to note that this involves very subtle changes in the character of NO. The frequency of the NO fundamental transition of ClNO ranges from 1805 to 1869 cm^{-1} in the solvents studied here, but the fundamental frequency of NO^+ in acetonitrile is 2355 cm^{-1}. Even in the most polar solvent studied, the N−Cl bond distance is still close enough that it does not allow for complete electron transfer.

The notable increase in the vibrational frequency of the NO-stretch fundamental is accompanied by a significant increase in line width and change in line shape. In going from cyclohexane to acetonitrile, the 11 cm^{-1} fwhm Lorentzian transition picks up considerable Gaussian character and increases to 55 cm^{-1} fwhm. An increase in the width of the vibronic A-band of ClNO has previously been explained as an increase in the homogeneous linewidth of ClNO when comparing cyclohexane to acetonitrile. For this transition the homogeneous linewidth (Γ) is composed of two components: the excited state vibrational lifetime and solvent-induced pure dephasing. It is likely that the increase in width of the NO stretch in more polar environments arises from enhancement of the vibrational-relaxation rate, and also an increase in the distribution of NO bond strengths corresponding to increases in homogeneous and inhomogeneous broadening, respectively. It is important to note that the ground state energetics of ClNO are environment dependent and our TRIR studies provide insight as to the extent these modifications perturb the reaction dynamics.

ClNO Photochemistry in Solution. Photochemical studies of gaseous ClNO have found that direct dissociation to form Cl and NO is the dominant photoproduct channel following A-band photoexcitation.[42,43,45−54] Furthermore, the NO photofragment is produced with significant vibrational energy, with population of states as high as $n = 7$ observed following 337-nm photoexcitation.[25,44,51−53,55] A strikingly different picture emerges in low-temperature matrixes, where studies have shown the structural isomer (ClON) to be the only photoproduct formed.[12,56] In solution, the case is less clear. Resonance Raman intensity analysis studies of ClNO in cyclohexane and acetonitrile found evidence of modest excited state evolution along the NO stretch coordinate.[57,58] This observation suggests that the excited state of ClNO, and correspondingly the photochemistry derived from this state, is considerably modified in solution relative to the gas phase. In an effort to further elucidate the environment-dependent photochemistry of ClNO, UV pump−probe experiments of ClNO in acetonitrile and chloroform were performed.[38] Evidence for geminate recombination and photoproduct formation in both solvents was observed; however, quantification and assignment of the photochemical species produced was difficult to ascertain from the transient optical density evolution. However, these earlier studies provide an important point of contact for our own effort to investigate the geminate recombination quantum yield, vibrational excitation, and photoproduct assignment following photoexcitation of the A-band of ClNO in acetonitrile.

Geminate Recombination. In the UV pump−probe study of ClNO, 93% recovery of initially depleted ClNO based on observed optical-density evolution at 256 nm was reported. However, with the uncertainty in photoproduct locations and band widths this number was taken as an upper limit for geminate recombination. Further investigating this issue, the measured optical density change as a function of probe wavelength at 50 ps was reproduced assuming direct dissociation to Cl and NO as the predominant pathway and a quantum yield for Cl production of 0.55. The results presented here are consistent with this analysis. Specifically, although the observed

evolution in optical density across the band demonstrates a range of recoveries, from 30 to 56%, analysis of the photoproduct-free probe wavelengths yields a geminate recombination quantum yield of 0.54 ± 0.06, consistent with the pump−probe results.

Vibrational Energy Deposition. The studies presented here provide insight into the extent of vibrational excitation accompanying the reformation of ClNO via geminate recombination. Specifically, the 4-cm^{-1} experimental resolution combined with the significant anharmonicity of the NO stretch allow for a clear determination of excess vibrational energy deposition into the NO-stretch coordinate. The anharmonicity of the NO stretch remains relatively unperturbed with changes in environment: 18 in the gas phase, 17.5 in argon matrixes, and 18.75 ± 0.29 cm^{-1} in cyclohexane, carbon tetrachloride, chloroform, and dichloromethane. The $n = 1 \rightarrow 2$ transition is therefore predicted to be at 1836 cm^{-1}. This transition, although overlapping the red edge of the fundamental transition, is well within the spectral region investigated here (Figure 3). However, there is little evidence for vibrationally excited ClNO. Vibrational relaxation in this case, in such a polar solvent, is expected to be very efficient and is not expected to present itself on a 50- to 100-ps timescale. The width of this transition (55 cm^{-1}) in acetonitrile supports this assertion, indicating that the vibrational lifetime is enhanced relative to cyclohexane. The static nature of the spectra on this timescale suggests that if excess vibrational energy is being deposited along this coordinate following geminate recombination the relaxation is fast enough to be obscured by the absorption of the solvent mode and the photoproduct within the first few picoseconds. Further, previous UV pump−probe studies reveal no evidence for vibrational relaxation on the 50- to 100-ps time scale and resonance Raman data show little to no evolution along this coordinate. While this observation is surprising given the extensive vibrational excitation of the NO photofragment observed in the gas phase, it is not entirely unexpected when one considers the evidence suggesting that the energetics and displacement of the potential energy surfaces are significantly modified in solution. Therefore, the time-resolved infrared studies further suggest that the excited state is significantly modified along the N−O stretch coordinate in condensed environments such that structural evolution along this coordinate is significantly restricted in solution. The photochemical impacts of this behavior are discussed below.

Photoproduct Production. Construction of the photoproduct absorption spectrum (Figure 5B) reveals a feature at 1860 cm^{-1} that persists out to the longest delays investigated demonstrating that the corresponding photoproduct is stable on the ∼100-ps timescale. Vibrationally excited ClNO does not absorb at 1860 cm^{-1}. Further, the efficiency of vibrational relaxation is expected to be high in such a polar solvent so the lack of evolution in the absorption band on ∼100-ps timescale suggests that the cause of the asymmetry in Figure 5A is not vibrational relaxation. Only two possibilities remain for the photoproduct: NO and the structural isomer ClON. In acetonitrile NO absorbs at 1870 cm^{-1}, inconsistent with the transition observed here. This leaves the isomer as the remaining possibility for the photoproduct. In argon matrixes, the NO stretch fundamental of ClON is observed at 1842 cm^{-1}, lying between the absorption of ClNO (1805 cm^{-1}) and that of free NO (1870 cm^{-1}).[12] Is assignment of the isomer to the observed photoproduct reasonable if one has to invoke an 18-cm^{-1} shift in the NO stretch transition of this species? In ClON, the Cl is predicted to be even more weakly bound to the NO with nearly complete transfer of the NO 2π electron to the singly occupied valence p orbital of the Cl. The Cl−O bond length is elongated relative to the Cl−N bond length of the parent, stretching from 1.973 to 2.228 Å, and the N−O bond length consequently contracts from 1.13 to 1.113 Å. The isomer is therefore even more likely to be responsive to changes in environment and exhibit bathochromic shifts similar to that observed in ClNO.

With assignment of the photoproduct to ClON, partitioning of photoproduct pathways can be performed. Hallou et al. have measured the extinction coefficient of the NO-stretch fundamental transition of ClON and ClNO in argon matrixes and found that the transition is 4.0(±0.5)-fold stronger in ClON relative to ClNO.[12] A comparison of the maximum depletion of ClNO to the maximum absorption of ClON can therefore estimate the extent of isomer formation and elucidate the partitioning of photoproduct pathways. This analysis reveals that only ∼7% of initially excited ClNO results in ClON production. With geminate recombination accounting for 54% of initially excited ClNO, the remaining ∼39% must go on to form Cl and NO. This partitioning is consistent with the results of earlier UV pump−probe studies from our laboratory where following 267-nm photoexcitation of ClNO in acetonitrile a broad photoproduct peak centered at 295 nm with a small shoulder at ∼330 nm was observed. Despite uncertainty in photoproduct positions and band widths, arguments were made that the main photoproduct peak corresponded to the Cl:acetonitrile charge-transfer complex. The observed offset in optical density at 50 ps was reproduced assuming that Cl and NO were the only photoproducts formed with a quantum yield $\Phi = 0.55$. Moreover, we propose that the small shoulder at 330 nm is due to the isomer, ClON. Even with ∼7% production, the isomer should appear due to its large absorption cross section, about 4 times that of ClNO in the UV.

Careful examination of the photoproduct spectrum (Figure 5B) reveals the presence of a weak absorption from 1820 to 1836 cm^{-1} that persists out to the longest delays investigated. This absorption lies in the region of the C−C stretch overtone of acetonitrile, and we propose that this feature corresponds to formation of the Cl:acetonitrile charge-transfer complex (CTC). In support of this, the evolution in optical density of the acetonitrile CN stretch following ClNO photoexcitation was measured. Centered at 2250 cm^{-1}, the CN-stretch is well removed from any transition corresponding to ClNO. Preliminary observations of the optical density evolution of the CN-stretch at 2240 and 2260 cm^{-1} following photolysis of ClNO at 266 nm are presented in Figure 6. The optical-density evolution that occurs between 0 to 1.5 ps arises from the optical response of the cell windows. However, this evolution is followed by a persistent optical-density offset that was not observed in either the CN-stretch or the CC-stretch overtone in neat acetonitrile samples. The offset is positive for both probe frequencies which span the CN-stretch transition, suggesting that the overall transition intensity has increased due to formation of the Cl:solvent CTC. This measurable perturbation provides not only a novel way to monitor formation of the Cl:solvent CTC, but also a way to obtain information regarding the structure of this transient species. By investigating multiple solvent modes, a picture of the interaction between Cl and solvent could emerge.

Environment-Dependent Photochemistry. Our laboratory has explored the solution phase photochemistry of halooxides, and in particular OClO.[7,8,14,17−23,36,37,58,65,66] It is interesting at this point to compare the chemistry of this species to that of ClNO. The geminate recombination quantum yield for OClO in acetonitrile following 401-nm excitation is 0.53 ± 0.16, almost identical with that of ClNO. Although it is tempting to propose

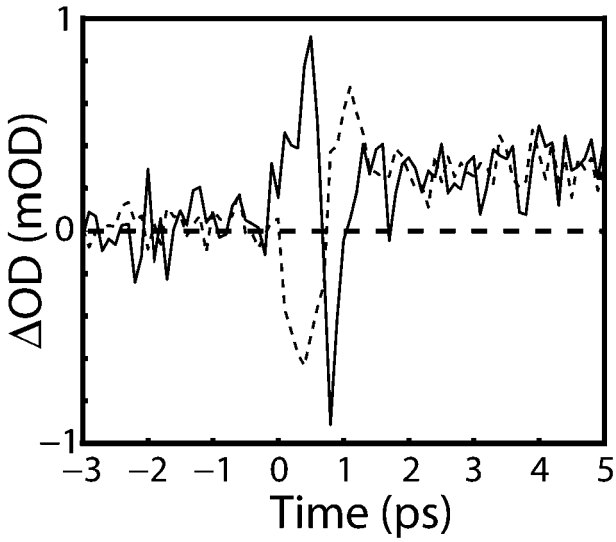

Figure 6. Evolution in optical density at 2240 cm^{-1} (solid line) and 2260 cm^{-1} (dashed line); 10 cm^{-1} to the red and the blue of the CN-stretch fundamental of acetonitrile, following photoexcitation of ClNO at 266 nm.

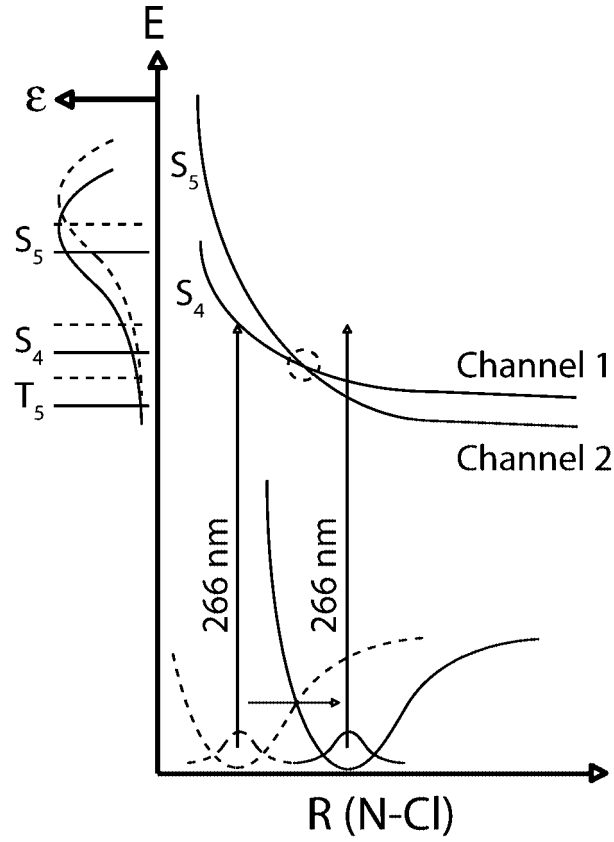

Figure 7. Dissociation scheme for ClNO. Dashed lines represent gas phase and solid lines represent a polar solvent environment. The plot of ε(E) on the left side presents the ClNO absorption spectra and expected energy of the electronic states. The avoided crossing between the S_5 and S_4 states is marked by a circle.

commonality in the photochemistry of these two species, it is important to keep in mind that the geminate recombination quantum yield of OClO is highly dependent on photolysis energy. Gas phase studies have demonstrated that more translational energy was imparted to the photofragments with increasing actinic energy, with increased translational energy translated into enhanced cage escape (that is, reduced geminate recombination) in solution. For ClNO, gas phase studies indicate that with increasing photolysis energy there is an increase in vibrational energy content of the NO fragment, and a slight decrease in translational energy imparted to the photofragments NO and Cl.[54] Skorokhodov et al. proposed that following A-band photoexcitation, two exit channels along the dissociative coordinate are accessed, and that these channels diverge at relatively short N−Cl bond distances. A schematic of the proposed dissociation is presented in Figure 7. In this model an avoided crossing of the S_5 and S_4 excited states is responsible for defining the two dissociative pathways. One pathway results in high translational energies imparted to the photoproducts with little excitation along the NO stretch. The other pathway results in less photoproduct translational energy and significantly more NO-stretch excitation. With increasing photolysis energy, Skorokhodov et al. observed an increase in the vibrational energy of the NO fragment, and a corresponding decrease in the translational energy of the Cl fragment. Recall, no evidence was found here for NO vibrational excitation following ClNO photolysis in acetonitrile in contrast to the behavior observed in the gas phase. Why would this be? In solution, the N−Cl bond length is elongated and the N−O bond length decreased in comparison to that of the gas phase. Resonance Raman studies of ClNO in cyclohexane and acetonitrile observed a weakened N−Cl bond in more polar solvents, corresponding to a shift of the ground state potential energy surface minimum along the reaction coordinate to larger N−Cl bond distances.[58] We propose that this shift results in preparation of the excited state beyond the avoided crossing such that the pathway corresponding to enhanced translational energy imparted to the photofragments is accessed and minimal NO vibrational excitation occurs. This hypothesis can be tested by comparative studies in nonpolar solvents where the ground state potential-energy-surface minimum should shift to shorter N−Cl bond lengths resulting in optical preparation of the excited state such that the vibrational-energy deposition into NO is increased.

Conclusions

We have performed FTIR studies of ClNO dissolved in cyclohexane, carbon tetrachloride, chloroform, dichloromethane, and acetonitrile. The spectra demonstrate that the energetics of the NO-stretch fundamental transition are highly solvent dependent. Specifically, the transition displays a linear shift to higher peak frequencies and significantly broadens with increasing solvent polarity. This solvent dependence is due to more efficient transfer of the 2π antibonding electron of NO to the valence p orbital of Cl in higher polarity solvents. Subsequently the NO fundamental exhibits enhanced vibrational relaxation rates and an increase in the distribution of NO bond energies.

We also performed the first TRIR investigation of ClNO in solution. Following 266-nm photoexcitation of ClNO in acetonitrile, the evolution in optical density in the photoproduct-free region of the band demonstrates a consistent geminate recombination quantum yield of 0.54 ± 0.06. The transient absorption spectra also reveal the instrument-response limited appearance of a photoproduct centered at 1860 cm^{-1}, and we have assigned this feature to formation of the structural isomer, ClON. By using the relative extinction coefficients for the NO stretch in ClON to ClNO, the quantum yield for isomer production is ~0.07. Little evidence is observed for significant vibrational excitation along the NO-stretch coordinate, this observation being consistent with previous resonance Raman studies that demonstrated the energetics and displacement of the ground and

excited states are significantly modified in solution relative to the gas phase.

We have proposed a scheme for the photodissociation process in solution derived from the proposal of Skorokhodov et al. wherein there are two photoproduct channels that arise from an avoided crossing of the S_5 and S_4 excited states. With increasing solvent polarity, improved solvation of the $Cl^{\delta-}$ and $NO^{\delta+}$ moieties consequently increases the N−Cl bond distance. Enhanced charge transfer from the NO antibonding 2π orbital to the valence p orbital of Cl shifts the ground state potential energy minimum along the reaction coordinate to longer N−Cl bond distances such that upon photoexcitation the product channel corresponding to minimal NO-stretch excitation is accessed.

Acknowledgment. The National Science Foundation (CHE-0350191) is acknowledged for their support of this work.

References and Notes

(1) Rowland, F. S. *Annu. Rev. Phys. Chem.* **1991**, *42*, 731.
(2) Renard, J. B.; Pirre, M.; Robert, C.; Huguenin, D. *J. Geophys. Res., [Atmos.]* **1998**, *103*, 25383.
(3) Solomon, S.; Borrmann, S.; Garcia, R. R.; Portmann, R.; Thomason, L.; Poole, L. R.; Winker, D.; McCormick, M. P. *J. Geophys. Res., [Atmos.]* **1997**, *102*, 21411.
(4) Donsig, H. A.; Herridge, D.; Vickerman, J. C. *J. Phys. Chem. A* **1998**, *103*, 9211.
(5) Fussen, D.; Valhellemont, F.; Dodion, J.; Bingen, C.; Mateshvili, N.; Daerden, F.; Fonteyn, D.; Errera, Q.; Chabrillat, S.; Kyrola, E.; Tamminen, J.; Sofievea, V.; Hauchercorne, A.; Dalaudier, F.; Bertaux, J.-L.; Renard, J.-B.; Fraisse, R.; d'Andon, O. F.; Barrot, G.; Guirlet, M.; Mangin, A.; Fehr, T.; Snoeij, P.; Saaverdra, L. *Geophys. Res. Lett.* **2006**, *33*, L13815.
(6) Vaida, V.; Simon, J. D. *Science* **1995**, *268*, 1443.
(7) Reid, P. J. *J. Phys. Chem. A* **2002**, *106*, 1473.
(8) Cooksey, C. C.; Reid, P. J. *Photochem. Photobiol.* **2004**, *80*, 386.
(9) Arkell, A.; Schwager, I. *J. Am. Chem. Soc.* **1967**, *89*, 5999.
(10) Rochkind, M. M.; Pimentel, G. C. *J. Chem. Phys.* **1967**, *46*, 4481.
(11) Holger, S.; Mueller, H. S. P.; Willner, H. *J. Phys. Chem.* **1993**, *97*, 10589.
(12) Hallou, A.; Schriver-Mazzuoli, L.; Schriver, A.; Chaquin, P. *Chem. Phys.* **1998**, *237*, 251.
(13) Thogersen, J.; Jepsen, P. U.; Thomsen, C. L.; Poulsen, J. A.; Byberg, J. R.; Keiding, S. R. *J. Phys. Chem. A* **1997**, *101*, 3317.
(14) Philpott, M. J.; Charalambous, S.; Reid, P. J. *Chem. Phys. Lett.* **1997**, *281*, 1.
(15) Thogersen, J.; Thomsen, C. L.; Poulsen, J. A.; Keiding, S. R. *J. Phys. Chem. A* **1998**, *102*, 4186.
(16) Poulsen, J. A.; Thomsen, C. L.; Keiding, S. R.; Thogersen, J. *J. Chem. Phys.* **1998**, *108*, 8461.
(17) Philpott, M. J.; Hayes, S. C.; Reid, P. J. *Chem. Phys.* **1998**, *236*, 207.
(18) Hayes, S. C.; Philpott, M. J.; Reid, P. J. *J. Chem. Phys.* **1998**, *109*, 2596.
(19) Hayes, S. C.; Philpott, M. P.; Mayer, S. G.; Reid, P. J. *J. Phys. Chem. A* **1999**, *103*, 5534.
(20) Thomsen, C. L.; Philpott, M. P.; Hayes, S. C.; Reid, P. J. *J. Chem. Phys.* **2000**, *112*, 505.
(21) Thomsen, C. L.; Reid, P. J.; Kieding, S. R. *J. Am. Chem. Soc.* **2000**, *122*, 12795.
(22) Philpott, M. J.; Hayes, S. C.; Thomsen, C. L.; Reid, P. J. *Chem. Phys.* **2001**, *263*, 389.
(23) Hayes, S. C.; Thomsen, C. L.; Reid, P. J. *J. Chem. Phys.* **2001**, *115*, 11228.
(24) Edgecombe, F. H. C.; Norrish, R. G. W.; Thrush, F. R. S.; Thrush, B. A. *Proc. R. Soc. London A* **1957**, *243*, 24.
(25) Basco, N.; Dogra, S. K. *Proc. R. Soc. London A* **1971**, *323*, 401.
(26) Sander, S. P.; Friedl, R. R. *J. Phys. Chem.* **1989**, *93*, 4764.
(27) Chichinin, A. I. *Chem. Phys. Lett.* **1993**, *209*, 459.
(28) Nelson, C. M.; Moore, T. A.; Okumura, M.; Minton, T. K. *J. Chem. Phys.* **1994**, *100*, 8055.
(29) Nickolaisen, S. L.; Miller, C. E.; Sander, S. P.; Hand, M. R.; Williams, I. H.; Francisco, J. S. *J. Chem. Phys.* **1996**, *104*, 2857.
(30) Moore, T. A.; Okumura, M.; Minton, T. K. *J. Chem. Phys.* **1997**, *107*, 3337.
(31) Tanaka, Y.; Kawasaki, M.; Matsumi, Y.; Fujiwara, H.; Ishiwata, T.; Rogers, L. J.; Dixon, R. N.; Ashfold, M. N. R. *J. Chem. Phys.* **1998**, *109*, 1315.
(32) Smith, G. D.; Tablas, F. M. G.; Molina, L. T.; Molina, M. J. *J. Phys. Chem. A* **2001**, *105*, 8658.
(33) Chi, F. K.; Andrews, L. *J. Phys. Chem.* **1973**, *77*, 3062.
(34) Johnsson, K.; Engdahl, A.; Nelander, B. *J. Phys. Chem.* **1995**, *99*, 3965.
(35) Gane, M. P.; Williams, N. A.; Sodeau, J. R. *J. Chem. Soc., Faraday Trans.* **1997**, *93*, 2747.
(36) Esposito, A. P.; Reid, P. J.; Rousslang, K. W. *J. Photochem. Photobiol., A* **1999**, *129*, 9.
(37) Cooksey, C. C.; Reid, P. J. *J. Phys. Chem. A* **2003**, *107*, 5508.
(38) Cooksey, C. C.; Johnson, K. J.; Reid, P. J. *J. Phys. Chem. A* **2006**, *110*, 8613.
(39) Luick, T.; Heckert, R.; Schulz, K.; Disselkamp, R. *J. Atmos. Chem.* **1999**, *32*, 315.
(40) Goodeve, C. F.; Katz, S. *Proc. R. Soc. A* **1939**, *172*, 432.
(41) Ballash, N. M.; Armstrong, D. A. *Spectrochim. Acta* **1974**, *30A*, 941.
(42) Colburn, C. B. *Developments in Inorganic Nitrogen Chemistry*; Elsevier Scientific Publishing Company: New York, 1973.
(43) Engelman, R.; Rouse, P. E. *J. Mol. Spectrosc.* **1971**, *37*, 240.
(44) Moser, M. D.; Weitz, E.; Schatz, G. C. *J. Chem. Phys.* **1983**, *78*, 757.
(45) Bechara, J.; Morrow, T.; McGrath, W. D. *Chem. Phys. Lett.* **1985**, *122*, 605.
(46) Ticktin, A.; Bruno, A. E.; Bruhlmann, U.; Huber, J. R. *Chem. Phys.* **1988**, *125*, 403.
(47) Bai, Y. Y.; Ogai, A.; Qian, C. X. W.; Iwata, L.; Segal, G. A.; Reisler, H. *J. Chem. Phys.* **1989**, *90*, 3903.
(48) Qian, C. X. W.; Ogai, A.; Iwata, L.; Reisler, H. *J. Chem. Phys.* **1990**, *92*, 4296.
(49) Ogai, A.; Qian, C. X. W.; Reisler, H. *J. Chem. Phys.* **1990**, *93*, 1107.
(50) Cao, J. Y.; Wang, Y. F.; Qian, C. X. W. *J. Chem. Phys.* **1995**, *103*, 9653.
(51) Haas, B. M.; Felder, P.; Huber, J. R. *Chem. Phys. Lett.* **1991**, *180*, 293.
(52) Gillan, I. T. F.; Denvir, D. J.; Cormican, H. F. J.; Duncan, I.; Murrow, T. *Chem. Phys.* **1992**, *167*, 193.
(53) Felder, P.; Morley, G. P. *Chem. Phys.* **1994**, *185*, 145.
(54) Skorokhodov, V.; Sato, Y.; Suto, K.; Matsumi, Y.; Kawasaki, M. *J. Phys. Chem.* **1996**, *100*, 12321.
(55) Werner, L.; Wunderer, B.; Walther, H. *Chem. Phys.* **1981**, *60*, 109.
(56) Maier, G.; Reisenauer, H. P.; De Marco, M. *Chem.-Eur. J.* **2000**, *6*, 800.
(57) Barham, B. P.; Reid, P. J. *Chem. Phys. Lett.* **2002**, *361*, 49.
(58) Nyholm, B. P.; Reid, P. J. *J. Phys. Chem. B* **2004**, *108*, 8716.
(59) Bell, A. J.; Frey, J. G. *Mol. Phys.* **1990**, *69*, 943.
(60) Mackey, J. L.; Johnson, B. R.; Kittrell, C.; Le, L. D.; Kinsey, J. L. *J. Chem. Phys.* **2001**, *114*, 6631.
(61) Jones, L. H.; Swanson, B. I. *J. Phys. Chem.* **1991**, *95*, 86.
(62) Schriver-Mazzuoli, L.; Hallou, A. S., A. *J. Phys. Chem. A* **1998**, *102*, 9772.
(63) Meredith, C.; Quelch, G. E.; Schaeffer, H. F. *J. Chem. Phys.* **1992**, *96*, 480.
(64) Lee, T. J. *J. Chem. Phys.* **1993**, *99*, 9783.
(65) Bolinger, J. C.; Bixby, T. J.; Reid, P. J. *J. Chem. Phys.* **2005**, *123*, 084503.
(66) Wallace, P. M.; Bolinger, J. C.; Hayes, S. C.; Reid, P. J. *J. Chem. Phys.* **2003**, *118*, 1183.

JP8100283